8-1-2023

Resolvin D1 prevents injurious neutrophil swarming in transplanted lungs

Wenjun Li
Washington University School of Medicine in St. Louis
Hailey M Shepherd
Washington University School of Medicine in St. Louis
Yuriko Terada
Washington University School of Medicine in St. Louis
Ashley E Shay
Harvard University
Amit I Bery
Washington University School of Medicine in St. Louis

See next page for additional authors

PNAS RESEARCH ARTICLE | IMMUNOLOGY AND INFLAMMATION

Resolvin D1 prevents injurious neutrophil swarming in transplanted lungs

Wenjun Li[a,1], Hailey M. Shepherd[a,1], Yuriko Terada[a], Ashley E. Shay[b], Amit I. Bery[c], Andrew E. Gelman[a,d], Kory J. Lavine[c], Charles N. Serhan[b], and Daniel Kreisel[a,d,2]

Edited by János G. Filep, Universite de Montreal, Montreal, Canada; received February 21, 2023; accepted June 27, 2023 by Editorial Board Member Carl F. Nathan

Neutrophils are the primary cell type involved in lung ischemia-reperfusion injury (IRI), which remains a frequent and morbid complication after organ transplantation. Endogenous lipid mediators that become activated during acute inflammation-resolution have gained increasing recognition for their protective role(s) in promoting the restoration of homeostasis, but their influence on early immune responses following transplantation remains to be uncovered. Resolvin D1, 7*S*,8*R*,17*S*-trihydroxy-4*Z*,9*E*,11*E*,13*Z*,15*E*,19*Z*-docosahexaenoic acid (RvD1), is a potent stereoselective mediator that exhibits proresolving and anti-inflammatory actions in the setting of tissue injury. Here, using metabololipidomics, we demonstrate that endogenous proresolving mediators including RvD1 are increased in human and murine lung grafts immediately following transplantation. In mouse grafts, we observe lipid mediator class switching early after reperfusion. We use intravital two-photon microscopy to reveal that RvD1 treatment significantly limits early neutrophil infiltration and swarming, thereby ameliorating early graft dysfunction in transplanted syngeneic lungs subjected to severe IRI. Through integrated analysis of single-cell RNA sequencing data of donor and recipient immune cells from lung grafts, we identify transcriptomic changes induced by RvD1. These results support a role for RvD1 as a potent modality for preventing early neutrophil-mediated tissue damage after lung IRI that may be therapeutic in the clinics.

inflammation | leukocytes | specialized proresolving mediators | lipid mediators | transplantation

Despite tremendous advancements in the field of organ transplantation over the past six decades, early graft dysfunction continues to represent a frequent complication after pulmonary transplantation with significant impact on short- and long-term outcomes (1). This manifests clinically as a syndrome termed primary graft dysfunction (PGD), which is characterized by leaking alveolar capillaries that results in radiographic pulmonary edema and impaired oxygenation within the first 72 h after lung transplantation (1). We and others have shown that neutrophils play a pivotal role in the pathogenesis of lung IRI (2, 3). One hallmark of IRI is damage to the capillary endothelium with vascular leakage, which we have recently demonstrated to be directly mediated by infiltrating recipient neutrophils (2). Using intravital microscopy, our work has revealed that a complex cross talk exists between donor and recipient immune cells that orchestrates neutrophil trafficking into reperfused lung grafts (4, 5). In response to damage-associated molecular patterns (DAMPs) released from graft cells that undergo necroptosis, donor nonclassical monocytes secrete neutrophil chemokines which recruit neutrophils to reperfused lungs (4). Subsequently, recipient classical monocytes mediate neutrophil extravasation through production of IL-1β that depends on MyD88 signaling (6). In addition to promoting early injury neutrophils interact with other immune cells within lung grafts, which can trigger graft rejection (6, 7). While perioperative neutrophil depletion attenuates IRI after lung transplantation in mice, this strategy is impractical in humans as these cells are essential for proper immune surveillance and clearance of invading pathogens. Hence, understanding the regulatory mechanisms involved in the resolution of the acute inflammatory response, without immune suppression jeopardizing the innate immune system's ability to combat microbial invaders (8), is critical to minimize IRI-mediated graft injury.

A novel superfamily of immunoregulatory lipid mediators known as the specialized proresolving mediators (SPMs) are potent local regulatory molecules biosynthesized during acute inflammation that serve to counterregulate proinflammatory mediator responses and actively promote resolution (8). Examples include docosahexaenoic acid (DHA)-derived (D-series resolvins, protectins, maresins), eicosapentaenoic acid (EPA)-derived (E-series resolvins), and arachidonic acid (AA)-derived (lipoxins) mediators (8). These lipid autocoids

Significance

Specialized endogenous lipid mediators are potent regulators of leukocyte responses that orchestrate key signaling pathways to promote resolution of inflammation and injury. Using metabololipidomics, we report that biosynthesis of endogenous proresolving mediators is up-regulated following reperfusion in human and mouse lung grafts. Intravital two-photon imaging and single-cell RNA sequencing reveal that treatment with RvD1 exerts protective effects on IRI after lung transplantation by decreasing neutrophil recruitment and swarming as well as attenuating expression of inflammatory genes by immune cells within the graft. These findings provide valuable insight for therapeutically enhancing proresolving pathways to minimize early leukocyte-mediated tissue injury and promote healing following transplantation.

This article is a PNAS Direct Submission. J.G.F. is a guest editor invited by the Editorial Board.

[1]W.L. and H.M.S. contributed equally to this work.

[2]To whom correspondence may be addressed. Email: kreiseld@wustl.edu.

This article contains supporting information online at https://www.pnas.org/lookup/suppl/doi:10.1073/pnas.2302938120/-/DCSupplemental.

Published July 24, 2023.

are produced in a highly organized temporal fashion during defined intervals of the inflammatory response and exert a broad array of immunomodulatory actions by regulating innate and adaptive immune cell responses (8). Leukotriene B_4 (LTB_4) is a potent chemoattractant that also orchestrates the unique neutrophil functional response of swarming (9, 10). Results from several experimental studies using IRI models suggest that RvD1 may be protective, proposing putative mechanisms such as increasing the percentage of regulatory T cells or facilitating M2 macrophage polarization (11, 12). The influence of RvD1 on early neutrophil trafficking has not been assessed in organ transplantation (13).

In this report, we sought to investigate the role of RvD1 in protecting against IRI-mediated tissue injury. We took advantage of a recently developed model of severe IRI after lung transplantation in which neutrophils are key mediators of tissue damage and early graft dysfunction. Using metabololipidomics, we found that SPMs including RvD1 within human and mouse lung grafts were markedly increased following reperfusion, consistent with prior evidence that indicates protective proresolving mechanisms are activated in response to IRI (8, 14). Intravital imaging revealed that administration of RvD1 confers profound protective actions including limiting neutrophil recruitment, extravasation, and swarming behavior, thereby preserving early graft function. Single-cell RNA sequencing revealed significant transcriptomic changes in donor and recipient immune cells induced by RvD1. These findings provide the foundation for therapeutics to diminish early tissue damage following transplantation.

Results

Endogenous SPMs Rapidly Increase in Human Lung Graft Tissue Following Transplantation. To evaluate whether endogenous SPMs are biosynthesized in lungs after clinical lung transplantation, levels of proresolving lipid mediators within the tissue of human lung grafts were monitored before and approximately 2 h after reperfusion by liquid chromatography tandem mass spectrometry (LC-MS/MS). We identified selected ion chromatograms and characteristic ions present within the MS/MS spectra consistent with the production of D-series resolvins in these human lung tissues, including RvD1, 17(R)-Resolvin D1 (17*R*-RvD1), Resolvin D4 (RvD4), Resolvin D5 (RvD5), and Resolvin D6 (RvD6) (Fig. 1 *A*–*E* and *SI Appendix*, Fig. S1 *A*–*E*). Identification included matching retention time and an unbiased MS/MS library match of ≥70% fit to synthetic material (Fig. 1 *A*–*E* and *SI Appendix*, Fig. S1 *A*–*E*). In patients without PGD, we found that amounts of several D-series resolvins and the resolvin precursor, 17-hydroxy docosahexaenoic acid (17-HDHA), were increased within human lung grafts following reperfusion compared to prereperfusion levels (Table 1). Of interest, this increase in D-series resolvins was not apparent in lungs that developed severe PGD, where we did not observe increases in levels of several SPMs, namely RvD4, RvD5, and RvD6 (Table 2). These results indicate that specific lipid mediators can accumulate in graft tissues after lung transplantation, raising the possibility that they may have a role in modulating early injury.

Proresolving Lipid Mediators Ameliorate Acute Inflammatory Responses Following IRI in Lung Grafts. Given the central role of neutrophils in IRI-mediated graft dysfunction after lung transplantation, we next set out to evaluate whether SPMs play a role in attenuating their early responses. We first generated a mixture of SPMs that have previously been shown to protect against tissue injury in other models (13–15), consisting of RvD1, lipoxin B_4 (LXB_4), RvE4, maresin 1 (MaR1), and protectin D1 (PD1). We transplanted B6 lungs into syngeneic LysM-GFP (green fluorescent protein) recipients that received this mixture of SPMs or vehicle control immediately prior to engraftment. As reported by our group and others, these mice allow neutrophils (bright green, GFP^{high}) to be distinguished from monocytes (dim green, $GFP^{intermediate}$) during intravital imaging (3, 16). To this end, the vast majority of GFP^{high} cells after transplantation of B6 lungs into B6 LysM-GFP mice have a phenotype consistent with infiltrating neutrophils (SSC^{high}, $CD11b^{high}$, $Ly6G^{high}$, $CD115^{-}$) (*SI Appendix*, Fig. S2). We utilized a model of severe IRI where lung grafts are exposed to both cold (60 min at 4 °C) and warm ischemic storage (45 min at 28 °C) where we have shown that early damage is dependent on neutrophilic infiltration (2, 17). This model is clinically relevant due to the rising prevalence of organ procurement from donors after circulatory death, which introduces a period of warm ischemia to the donor organ after circulation has ceased (18). Consistent with our earlier report, neutrophil swarming with formation of large aggregates was observed in the subpleural space under control conditions (Fig. 2*A* and Movie S1) (12). In contrast, lung grafts of recipients treated with the SPM mixture demonstrated a drastically reduced density of neutrophils, decreased extravasation and swarming, increased intravascular crawling velocities, as well as increased displacement (Fig. 2 *B*–*F* and Movie S2).

Resolvin D1 Attenuates Neutrophil Trafficking into Injured Lung Grafts and Protects Against Early Graft Dysfunction. Based on the protective effect of the SPM mixture and our previous reports showing RvD1-mediated organ protection (19), we next investigated the serial expression of RvD1 within lung graft tissue using our mouse model. We quantified endogenous levels of RvD1, its epimer, 17*R*-RvD1, as well as its precursor, 17-HDHA, using LC-MS/MS analysis. Immediately after reperfusion, we found that levels of all three lipid compounds were significantly increased in lung graft tissues (Fig. 3*A* and *SI Appendix*, Fig. S3), with a trend toward subsequent decreases. Additionally, we measured levels of prostaglandin E2 (PGE2), prostaglandin D2 (PGD2), and LTB_4 in lung grafts at the same time points after transplantation (Fig. 3 *B*–*D*). We found that levels of LTB_4 were significantly increased at 3 h after reperfusion with subsequent decreases, while PGD2 levels were significantly increased at 7 d compared to baseline. We next investigated whether treatment with exogenous RvD1 impacted innate immune cell recruitment and graft function. While the abundance of recipient classical monocytes recruited to the transplanted lung was comparable between vehicle and RvD1 treatment, we observed a significant decrease in the abundance of recipient neutrophils after treatment with RvD1 (Fig. 4 *A*–*C*). Thus, the ratio of recruited neutrophils to classical monocytes is decreased after RvD1 treatment. Similar to treatment with the mixture of SPMs, monotherapy with RvD1 resulted in significantly reduced neutrophil recruitment and swarming behavior (Fig. 4 *D* and *E* and Movie S3). We observed significantly decreased neutrophil cell densities, reduced extravasation, increased displacement, and increased intravascular crawling velocities with RvD1 treatment compared to vehicle (Fig. 4 *F*–*I* and Movies S4 and S5). In comparison to vehicle-treated lung grafts in which neutrophils were observed to have multidirectional trafficking, often migrating opposite to the direction of the blood flow, neutrophils within RvD1-treated grafts exhibited linear trafficking in the same direction as the blood flow (Movies S4 and S5). This modulation in neutrophil trafficking was associated with significantly improved early graft function (Fig. 4*J*). We did not observe alterations in LTB_4 levels

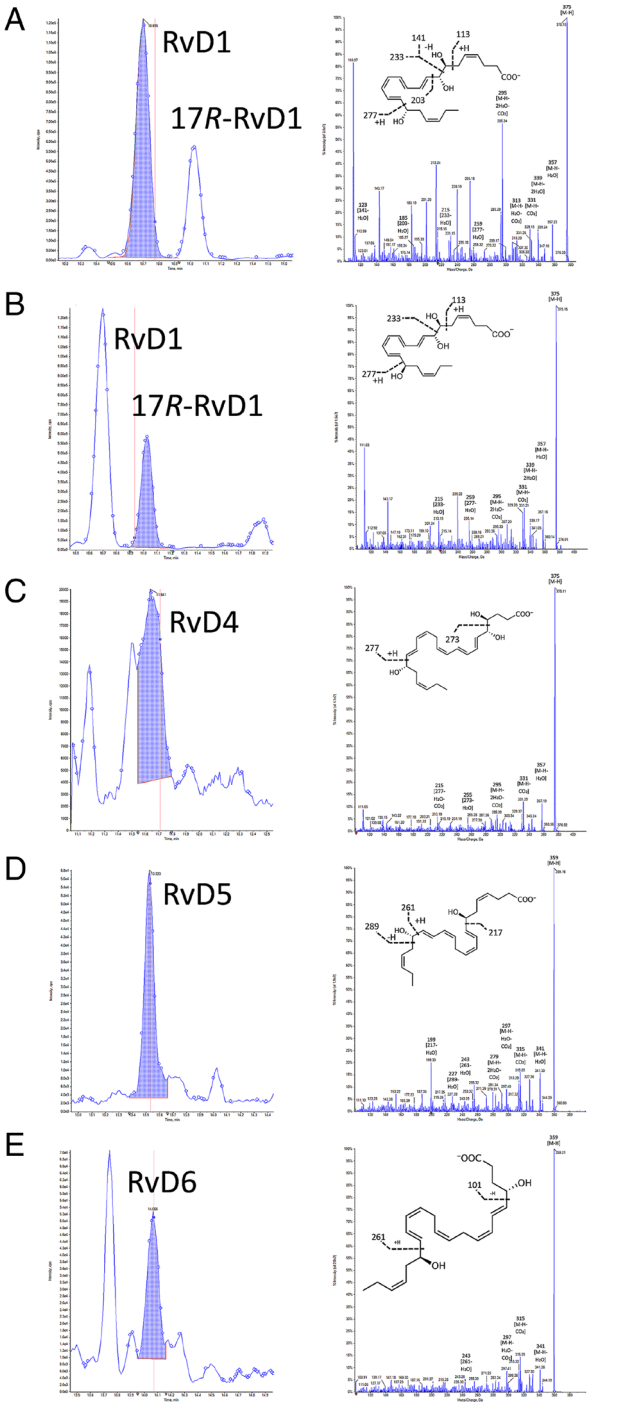

Fig. 1. LC-MS/MS identification of RvD1 in reperfused human lung grafts. (*A–E*) LC-MS/MS identification of SPMs in transplanted human lungs following reperfusion. (*A*) MRM for RvD1 (*A*, *Left*) *m/z* 375 > 215, enhanced product ion (EPI) spectra (*A*, *Right*), and RvD1 structure with fragmentation (*A*, *Right Inset).* RvD1 had an 89.9% fit to authentic RvD1 in a custom metabololipidomics spectral library. (*B*) MRM for 17*R*-RvD1 (*B, Left*) *m/z* 375 > 215, EPI spectra (*B*, *Right*), and 17*R*-RvD1 structure with fragmentation (*B*, *Right Inset).* 17*R*-RvD1 had a 77.2% fit to authentic 17*R*-RvD1 in a custom metabololipidomics spectral library. (*C*) MRM for RvD4 (*C*, *Left*) *m/z* 375 > 101, EPI spectra (*C*, *Right*), and RvD4 structure with fragmentation (*C*, *Right Inset).* RvD4 had an 88.4% fit to authentic RvD4 in a custom metabololipidomics spectral library. (*D*) MRM for RvD5 (*D*, *Left*) *m/z* 359 > 199, EPI spectra (*D*, *Right*), and RvD5 structure with fragmentation (*D*, *Right Inset*). RvD5 had a 91.6% fit to authentic RvD5 in a custom metabololipidomics spectral library. (*E*) MRM for RvD6 (*E*, *Left*) *m/z* 359 > 101, EPI spectra (*E*, *Right*), and RvD6 structure with fragmentation (*E*, *Right Inset).* RvD6 had a 97.1% fit to authentic RvD6 in a custom metabololipidomics spectral library. The default values of 0.00th for *m/z* are shown. Note that the accuracy of this instrument is approximately ± 0.1 *m/z*. MRM chromatograms and EPI spectra are shown as screen captures from Sciex OS-Q software version 1.7.0.36606.

in the graft tissue at 3 h after reperfusion following treatment with RvD1 compared to vehicle (*SI Appendix*, Fig. S4).

RvD1-Treated Lung Grafts Exhibit Altered Transcriptional Profiles by Single-Cell RNA Sequencing. We have previously shown that neutrophil recruitment into lung grafts during IRI is mediated by chemokines produced by donor-derived nonclassical monocytes (4, 6). To elucidate the molecular mechanisms of RvD1's anti-inflammatory and proresolving actions within lung grafts, we next obtained single-cell RNA sequencing data of sorted $CD45^+$ leukocytes from transplanted lung grafts exposed to severe IRI 2 h after transplantation. From these data, we synthesized an integrated dataset consisting of 22,645 cells representing 11 major types of leukocytes (Fig. 5*A*). Individual cell clusters exhibited unique gene enrichment profiles and cell identities were validated by expression of canonical marker genes (Fig. 5*B* and *SI Appendix*, Fig. S5 *A* and *B*). The dataset was interrogated to investigate which cell populations expressed the RvD1 receptor, ALX/FPR2 (19), which was highly expressed by neutrophils, alveolar macrophages, and nonclassical monocytes (Fig. 5*C*). Based on these findings, we next evaluated the differential gene expression in these cell populations of RvD1—compared to vehicle-treated lungs. In all three populations, we found markedly altered gene expression profiles induced by RvD1 treatment, which correlated with down-regulated inflammatory signaling by pathway analysis (Fig. 5*D*). Given our previously reported findings of monocytic populations regulating neutrophil trafficking, we subset the myeloid populations within our global object and performed normalization and reclustering for further focused analysis. This myeloid subset contained 3,896 cells that included nonclassical monocytes, classical monocytes, macrophages, and dendritic cells, which were largely present in both treatment groups (Fig. 5 *E* and *F* and *SI Appendix*, Fig. S5*C*). Within this myeloid population, we noted expression of proinflammatory cytokines and chemokines (Fig. 5*G*). When compared between treatment groups, we observed significantly decreased CXCL2 and TNF-α expression in RvD1-treated lungs (Fig. 5*H*).

Discussion

Here, we report that endogenous SPMs are present within human and mouse lung tissue before and after transplantation with clinical correlation to early graft dysfunction. In mouse grafts, we observed that the lipid mediator class switch occurs early after lung transplantation with transient increases in LTB_4 levels soon after reperfusion and sustained elevation of RvD1 levels until at least day 7 (20, 21). We observe that RvD1 reduced the early recruitment and extravasation of neutrophils into lung grafts in a model of severe IRI, which was associated with improved graft function. We describe an integrated single-cell RNA sequencing dataset comparing vehicle and RvD1-treated transplanted lungs and characterize transcriptional changes induced by RvD1 that delineate putative mechanisms underlying its immunomodulation. Understanding protective regulatory pathways is essential to prevent or ameliorate IRI-mediated graft dysfunction and promote inflammation resolution following transplantation.

Work by our group and others have described the central role that neutrophils play in mediating early tissue damage after lung transplantation (2). Intravital imaging has shed new light on cellular and molecular requirements for neutrophil recruitment into injured lungs. Of note, cues that guide neutrophils into tissues during sterile inflammation differ between organs (22). We have described a role for chemokine and cytokine production by monocytes and macrophages in this process (2, 4, 5). Given the

Table 1. Quantification of D-series resolvins in human lung grafts prereperfusion and postreperfusion without PGD

	RvD1	17R-RvD1	RvD4	RvD5	RvD6	17-HDHA
Sample	pg/200 mg Lung					
Pre-perfusion #1	0.0	0.0	0.0	35.1	2.2	559.4
Pre-perfusion #2	0.0	6.7	0.0	22.2	0.8	1,201.8
Pre-perfusion #3	0.0	0.0	0.0	39.5	0.8	285.9
Pre-perfusion #4	289.9	182.5	0.0	5.9	2.0	455.2
Pre-perfusion #5	0.0	0.0	0.0	16.8	0.0	503.0
Post-perfusion #1	5,701.2	3,622.6	53.4	0.0	42.2	876.2
Post-perfusion #2	1,983.5	2,112.1	38	112.8	47.8	1,858.1
Post-perfusion #3	0.0	0.0	26.3	312.8	20.6	744.4
Post-perfusion #4	1,377.3	1,388.8	16.3	30.7	11.7	372.0
Post-perfusion #5	0.0	0.0	19.3	421.8	9.9	621.0

Quantification of RvD1, 17*R*-RvD1, RvD4, RvD5, RvD6, and 17-HDHA levels in human lung grafts prereperfusion and postreperfusion from patients without PGD. Data shown as pg/200 mg lung.

impractical nature inherent to neutrophil depletion in the clinics, it is desirable to devise therapeutic avenues that interrupt networks of inflammatory signaling leading to their recruitment. We and others have shown that therapy with SPMs exerts potent protective effects in various experimental models of inflammation (8). Notably, earlier results demonstrated that RvE1 regulates the expression of adhesion molecules on neutrophils and monocytes, which results in a reduced capacity to interact with vascular endothelium (23). Compared to vehicle-treated lungs, RvD1 treatment resulted in significantly increased neutrophil intraluminal crawling velocities. Following their adherence to the vessel walls, neutrophils crawl along the vascular endothelium prior to reaching their optimal extravasation sites (24). Therefore, alterations in crawling behavior can impair neutrophilic extravasation. To this end, it is possible that neutrophils use transcellular rather than paracellular routes to extravasate when crawling is impaired, which is a less efficient process. We also observed increases in intraluminal displacement after treatment with RvD1. Thus, intravascular administration of RvD1 disrupts intravascular steps that are critical to facilitate efficient neutrophil extravasation.

Using a cremaster muscle preparation, Phillipson and colleagues discovered that interactions between Mac-1 on neutrophils and ICAM-1 on endothelial cells promoted their crawling to their optimal emigration site, thereby facilitating efficient extravasation. Similarly, we have previously shown that inhibition of Mac-1 results in decreased neutrophil intravascular crawling velocities, decreased transendothelial migration velocity, and decreased extravascular velocities after heart transplantation (25). Therefore, it is possible that RvD1 alters neutrophilic crawling behavior by down-regulating expression of ICAM-1 on pulmonary vascular endothelium. To this end, RvD1-treated lung grafts showed decreased expression of TNF-α, a proinflammatory cytokine that has been linked to lung IRI. TNF-α is known to promote increased expression of adhesion molecules on vascular endothelial cells in injured lungs, which could enhance leukocyte recruitment (26). Also, TNF-α triggers the production of the neutrophil chemokine CXCL1 by airway epithelial cells (27). Our gene expression analysis revealed reduced expression of the neutrophil chemokine CXCL2 in monocytic populations. In prior studies, we have defined CXCL2 expression by donor nonclassical monocytes and donor alveolar macrophages as critical for neutrophil recruitment (4, 28). We have also found that graft infiltrating recipient classical monocytes express high levels of CXCL2, thereby potentially promoting neutrophil cluster formation within the graft (6). Previous studies have reported that RvD1 inhibits the synthesis of LTB_4, a lipid mediator of neutrophil chemokinesis (15). Also, prior reports have indicated that neutrophil-derived LTB_4 can play an important role in promoting extravascular neutrophil swarming (29). We did not detect reductions in tissue LTB_4 levels after RvD1 treatment, raising the possibility that RvD1 regulates neutrophil trafficking after lung transplantation through other mechanisms. However, our examination was limited to a single time point, and a temporal analysis may be warranted to further explore the impact of RvD1 on LTB_4 and other inflammatory mediators.

Table 2. Quantification of D-series Resolvins in human lung grafts prereperfusion and postreperfusion with PGD

	RvD1	17R-RvD1	RvD4	RvD5	RvD6	17-HDHA
Sample	pg/200 mg Lung					
Pre-perfusion #1	390.6	205.1	0.0	5.8	0.5	125.4
Pre-perfusion #2	50.1	4.5	0.0	165.6	0.8	2,000.1
Pre-perfusion #3	330.1	119.4	0.0	39.5	0.6	249.7
Pre-perfusion #4	0.0	28.6	0.0	77.4	0.8	750.5
Post-perfusion #1	465.4	209.6	0.0	2.3	0.0	136.4
Post-perfusion #2	0.0	0.0	2.0	2.0	0.0	158.2
Post-perfusion #3	809.3	448.2	1.2	2.8	0.5	161.2
Post-perfusion #4	0.0	0.0	0.7	1.6	0.0	110.5

Quantification of RvD1, 17*R*-RvD1, RvD4, RvD5, RvD6, and 17-HDHA levels in human lung grafts prereperfusion and postreperfusion from patients with PGD. Data shown as pg/200 mg lung.

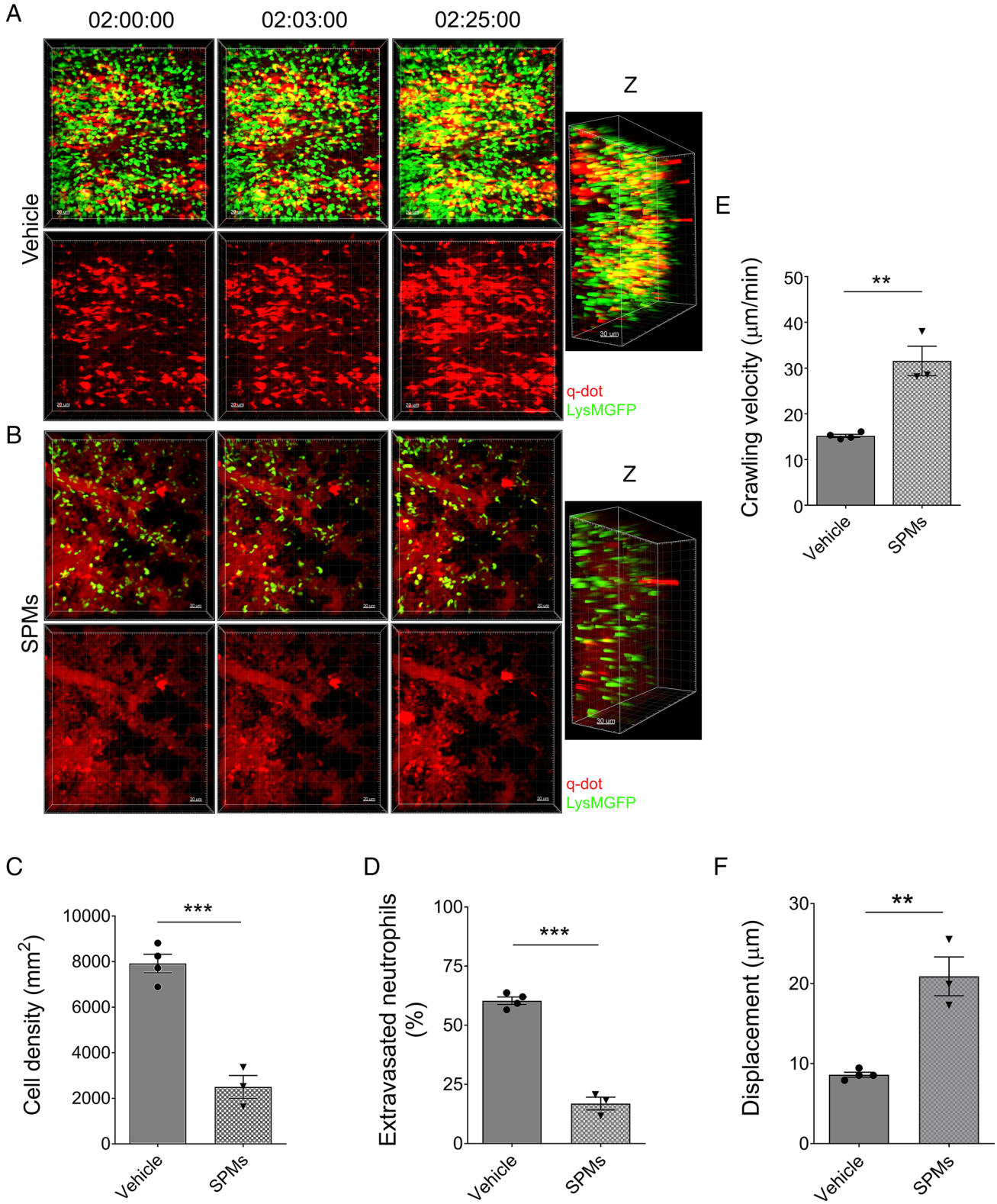

Fig. 2. SPMs significantly reduce neutrophil infiltration into reperfused lung grafts. (*A* and *B*) Time lapse intravital two-photon imaging of (*A*) vehicle-treated lung grafts and (*B*) SPM mixture (containing RvD1, LXB_4, RvE4, MaR1, and PD1)-treated lung grafts. Top panels depict infiltrating neutrophils (green) and bottom panels illustrate pulmonary microcirculation labeled with intravenous injection of quantum dots (red). Side projections of *z* stacks are shown. (*C*) Quantification of cell density of recipient GFP^+ neutrophils within lung grafts following treatment with vehicle or SPM mixture. (*D*) Percentage of extravasated recipient GFP^+ neutrophils in lung grafts following treatment with vehicle or SPM mixture. (*E*) Intraluminal crawling velocities and (*F*) displacement of recipient GFP^+ neutrophils following treatment with vehicle or SPM mixture. Significance of all data was compared using an unpaired two-tailed Student's *t* test. ***$P < 0.001$ **$P < 0.01$ compared to vehicle. Data in (*C*–*F*) represent mean ± SEM and $n = 3$ to 4 lungs per group.

These data expand upon other reports describing RvD1's protective effects during lung injury (13, 14, 30–33). For example, supplementation with RvD1 attenuates the development of cigarette smoke-induced emphysema (30). RvD1 blunted inflammatory responses in long-term cigarette smoke-exposed murine lungs, including reduced neutrophilic and macrophage infiltration.

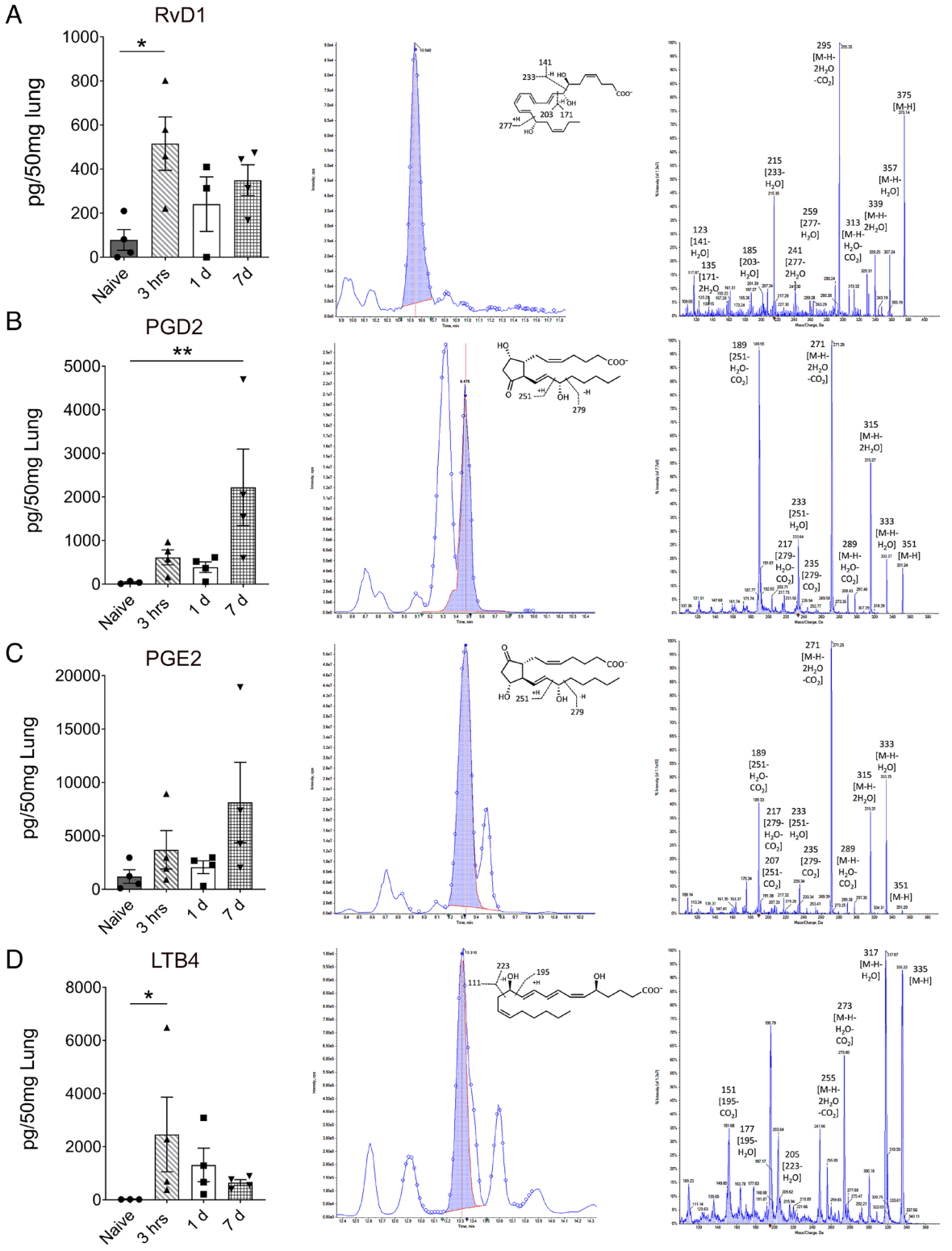

Fig. 3. Endogenous lipid mediators increase early after mouse lung graft reperfusion. *(A)* Quantification of RvD1 in mouse lung grafts over time (*A*, *Left*) MRM for m/z 375 > 215 (*A*, *Middle*), and enhanced product ion (EPI) spectra for RvD1 (*A*, *Right*) with an 87.6% fit to authentic RvD1 in a custom metabololipidomics spectral library. (*B*) Quantification of PGD2 in mouse lung grafts over time (*B*, *Left*), MRM for m/z 351 > 233, (*B*, *Middle*), and EPI spectra for PGD2 (*B*, *Right*) with a 99.7% fit to authentic PGD2 in a custom metabololipidomics spectral library. (*C*) Quantification of PGE2 in mouse lung grafts over time (*C*, *Left*), MRM for m/z 351 > 189 (*C*, *Middle*), EPI spectra for PGE2 (*C*, *Right*) with a 99.6% fit to authentic PGE2 in a custom metabololipidomics spectral library. (*D*) Quantification of LTB_4 in mouse lung grafts over time (*D*, *Left*), MRM for m/z 351 > 189 (*D*, *Middle*), EPI spectra for LTB_4 (*D*, *Right*) with a 98.3% fit to authentic LTB_4 in a custom metabololipidomics spectral library. *n* = 3 to 4 per group. Significance of the data was compared by Kruskal–Wallis test. *$P < 0.05$ **$P < 0.01$. MRM chromatograms and EPI spectra are shown as screen captures from Sciex OS-Q software version 1.7.0.36606.

RvD1 has also been shown to attenuate acute lung injury after inhalational exposure to LPS (31). The authors suggest that the RvD1 mechanism involves reduction in CXCL2 production by alveolar macrophages, which resulted in diminished neutrophilic infiltration on histological analysis. Moreover, the aspirin-triggered form of RvD1, 17*R*-RvD1, enhances clearance of gram-negative

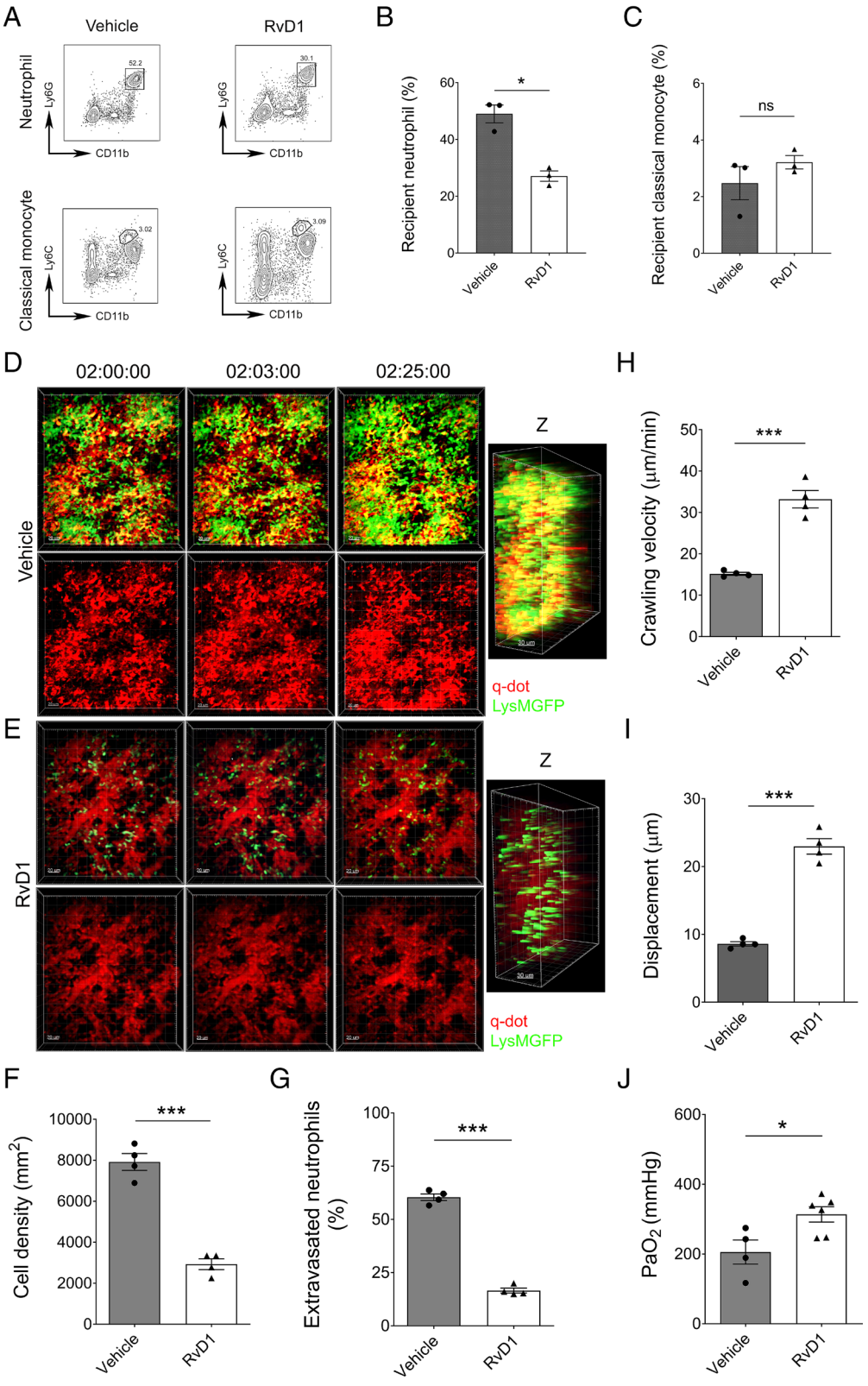

Fig. 4. RvD1 treatment significantly attenuates neutrophil recruitment and extravasation into injured lung grafts. (*A*) Contour plots depicting recipient neutrophils ($Ly6G^{high}$, $CD11b^{+}$) and classical monocytes ($Ly6C^{high}$, $CD11b^{+}$) 2 h after B6 CD45.1 B6 CD45.2 lung transplantation treated with vehicle or RvD1. Plots are gated on $CD45.1^{-}$, $CD45.2^{+}$ live (defined by forward side scatter characteristics) cells. (*B* and *C*) Quantification of abundance of recipient neutrophils (*B*) and recipient classical monocytes (*C*) in reperfused lung grafts treated with vehicle or RvD1 (as percentage of $CD45.1^{-}$ $CD45.2^{+}$ cells). (*D* and *E*) Time lapse intravital two-photon imaging of (*D*) vehicle-treated lung grafts and (*E*) RvD1-treated lung grafts. Top panels depict infiltrating neutrophils (green) and bottom panels illustrate pulmonary microcirculation labeled with intravenous injection of quantum dots (red). Side projections of *z* stacks are shown. (*F*) Quantification of cell density of recipient GFP^{+} neutrophils within lung grafts following treatment with vehicle or RvD1. (*G*) Percentage of extravasated recipient GFP^{+} neutrophils in lung grafts following treatment with vehicle or RvD1. (*H*) Intraluminal crawling velocities and (*I*) displacement of recipient GFP^{+} neutrophils following treatment with vehicle or RvD1. (*J*) Arterial blood oxygenation obtained 2 h after reperfusion of syngeneic lungs subjected to severe IRI in recipients treated with vehicle or RvD1. Significance of all data was compared using an unpaired two-tailed Student's *t* test. $*P < 0.05$ compared to vehicle. $***P < 0.001$ compared to vehicle. Data in (*B* and *C*) represent mean ± SEM ($n = 3$ lungs per group). Data in (*F–J*) represent mean ± SEM ($n = 4$ to 5 lungs per group).

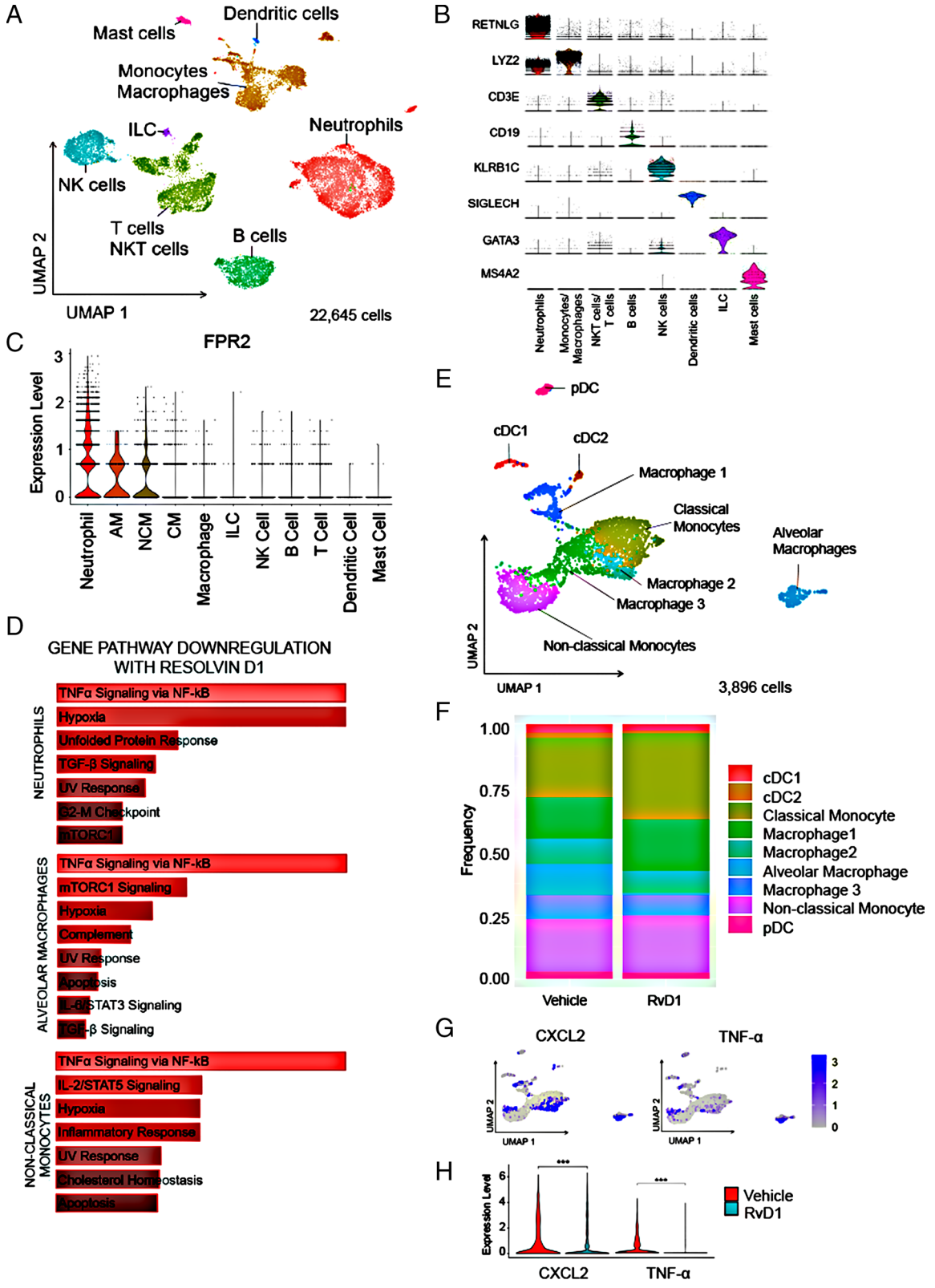

Fig. 5. Transcriptome profiling of lung graft immune cells by single-cell RNA sequencing. Single-cell RNA sequencing data from transplanted syngeneic mouse lungs following recipient treatment with intravenous RvD1 or vehicle immediately prior to transplantation. (*A*) Annotated cell types depicted in Unsupervised UMAP plot clustering of 22,645 cells after quality control and data filtering using Harmony integration. ILC: Innate lymphoid cell, NK cell: Natural Killer cell. (*B*) Violin plots generated from the integrated dataset illustrating canonical genes for each annotated cell population. (*C*) Violin plot showing FPR2 expression across cell populations. AM: alveolar macrophage, NCM: nonclassical monocyte, CM: classical monocyte. (*D*) MSigDB Hallmark 2020 Pathway analysis identifying top differentially down-regulated gene pathways in leukocytes from RvD1-treated lung grafts compared to vehicle. (*E*) Unsupervised reclustering of monocyte/macrophage cells within the integrated dataset with annotated cell types delineated. pDC: plasmacytoid dendritic cell, cDC1: conventional dendritic cell 1, cDC2: conventional dendritic cell 2. (*F*) Stack plot depicting composition of cell types within monocyte/macrophage subset between vehicle- and RvD1-treated lung grafts. (*G*) Feature plots illustrating CXCL2 (*Left*) and TNF-α (*Right*) expression across cell types in the monocyte/macrophage subset. (*H*) Violin plots demonstrating significantly reduced expression of CXCL2 (*Left*) and TNF-α (*Right*) expression in the monocyte/macrophage subset. Data are derived from two pooled lungs per condition. Pairwise comparisons using Wilcox test. ***$P < 0.001$.

bacteria after respiratory infections, which is at least in part due to enhanced phagocytosis by macrophages (32). Resolvin-enhanced efferocytosis was also shown to facilitate clearance of apoptotic neutrophils by macrophages, promoting the resolution of inflammation. More recently, two groups evaluated RvD1 in rodent models of lung IRI. In contrast to our observations in the mouse lung transplant model, Oda and colleagues reported that rat tissue levels of RvD1 decrease within 3 h after temporary clamping of the pulmonary hilum (14). Treatment of rats with aspirin-triggered RvD1 resulted in decreased tissue levels of IL-1β and IL-6, a lower density of neutrophils on immunohistochemical analysis, and improved lung function 3 h after reperfusion. These results are consistent with the present results (Fig. 4 and Movies S1–S3). Leroy and colleagues evaluated levels of SPMs in the airway fluid of human lung transplant recipients and mice that were subjected to transient occlusion of the pulmonary hilum (13). Both RvD1 and Mar1 were increased in the bronchoalveolar lavage fluid of lung transplant patients at 7 d, but not at 24 h after engraftment. Similar observations were made in their mouse pulmonary clamp model where increased levels of RvD1 and Mar1 were noted in airway fluid at 24, but not 6 h after reperfusion (12). These findings compare with our observations in human and mouse lung transplant recipients where the tissue levels of SPMs are increased substantially early after reperfusion. It is interesting to note that we have not observed higher levels of 17-HDHA relative to RvD1. It is likely that when biosynthesized in vivo 17-HDHA is rapidly esterified into phospholipids and/or other complex lipids that were not extracted in our solid phase extraction nor could be identified with the negative ion mode of our targeted LC-MS-MS method (34). Future studies will need to determine whether levels of SPMs in the airways are reflective of those in the lung tissue, as we posit that their protective action may be influenced by cells they engage in various compartments. Increased protective effects were observed at 6 h after lung clamping reperfusion and 24 h after lung transplantation when animals were treated with RvD1 and Mar1 compared to RvD1 or MaR1 alone. The authors suggest that RvD1 acts primarily on alveolar macrophages decreasing their production of inflammatory cytokines and chemokines and promoting their efferocytosis of apoptotic neutrophils, while MaR1 inhibits neutrophil chemokine production by airway epithelium. Our gene expression analysis demonstrated that several immune cells in lung grafts express the RvD1 receptor, ALX/FPR2, early after reperfusion, raising the possibility that RvD1 may regulate the function of various cells.

We have previously reported that inflammation during severe IRI after lung transplantation is initiated by necroptotic death of graft cells (2). Necroptosis results in lysis of the cell membrane and the release of DAMPs that can activate innate immune receptors. We have recently shown that levels of HMGB-1, an endogenous nucleoprotein that can bind to TLR4 and the receptor for advanced glycation end products (RAGE), are significantly increased in the systemic circulation early after reperfusion of the transplanted lung (2). HMGB-1 binding to RAGE on monocytes can induce the production of the proinflammatory lipid mediator LTB_4 (35). Interestingly, simultaneous stimulation with HMGB-1 and C1q, a component of the classical complement pathway that we have recently shown to be increased in lung transplant recipients who experience severe PGD, results in production of SPMs, including RvD1 (36). Another benefit of RvD1 treatment is its ability to enhance the clearance of necroptotic cells, for example by promoting fatty acid oxidation and oxidative phosphorylation in macrophages (37). Furthermore, recent work has demonstrated that resolvins can promote the clearance of neutrophil extracellular traps (NETs), which we and others have shown are associated with severe IRI after lung transplantation (2, 38). Thus, RvD1 exerts both anti-inflammatory and proresolution effects (39).

These observations have important implications for therapeutic considerations, since augmenting these responses would require intervention during the initial phase of vascular inflammation. Pharmacologic delivery via flushing organs or by utilizing ex vivo perfusion circuits could serve as unique opportunities for targeting these pathways in donor grafts prior to transplantation. In addition to inhibiting innate immune responses, RvD1 treatment may also blunt the alloimmune response, as we have previously shown that neutrophils can contribute to activation of T cells within lung grafts (7). Furthermore, such therapeutic methods could offer additional immunomodulatory benefits, such as promoting infection clearance and reducing antibiotic requirements (40). Given the protective benefits of resolvins and the safety associated with endogenous mediators, the present findings shed light on lipid mediators as an immunomodulatory therapy to minimize graft injury and promote inflammatory resolution following transplantation of lungs and possibly other organs and surgical procedures.

Materials and Methods

Mice. C57BL/6 (B6) wild type ($CD45.2^+$), and B6.SJL-PtprcaPepcb/BoyJ ($CD45.1^+$) were purchased from Jackson Laboratories. B6 LysM-GFP mice were originally obtained from Klaus Ley (Scripps) and provided by M. Miller (Washington University, St. Louis, MO). For all experiments, 6 to 8-wk-old male and female mice were used. Donor and recipient mice were gender-matched for all transplants. All animal procedures were approved by the Animal Studies Committee at Washington University School of Medicine. Animals received humane care in compliance with the "Guide for the care and use of laboratory animals" prepared by the National Academy of Sciences and published by the NIH and the "Principles of laboratory animal care" formulated by the National Society for Medical Research.

Human Samples. Human pulmonary graft samples were obtained during clinical lung transplants at the conclusion of cold ischemic storage in Perfadex solution and approximately 2 h after reperfusion. Samples were collected from patients with (Grade 3) and without PGD (Grade 0) for liquid chromatography tandem mass spectrometry analysis. Human protocols were approved by the Institutional Review Board at Washington University School of Medicine. Study subjects signed an informed consent.

Mouse Samples. Orthotopic left vascularized lung transplants were performed as previously described (17). Grafts were stored in low-potassium dextran glucose solution for 60 min at 4 °C with an additional 45 min at 28 °C prior to transplantation to induce severe IRI as previously described (2). In some experiments, recipients were treated with a proresolving cocktail consisting of five lipid mediators (RvD1, LXB_4, RvE4, MaR1, and PD1) administered intravenously immediately prior to transplantation (1.2 μg of each in 30 μL 100% ethanol, see *SI Appendix*, Table S2). Some recipients received intravenous administration of RvD1 (200 ng/per mouse in 200 μL 1% ethanol, Cayman Chemical Company, #10012554) or vehicle immediately before transplantation.

Targeted Liquid Chromatography Tandem Mass Spectrometry. Lung samples were incubated at −80 °C for at least 30 min with ice-cold LC-MS grade methanol (Thermo Fisher Scientific) containing 500 pg of each of the following: d5-RvD2, d5-RvD3, d5-LXA_4, d5-MaR1, d4-LTB_4, d8-15S-HETE, and d8-5S-HETE (Cayman Chemical) for calculating quantification and recovery. Samples were extracted as described in ref. 41. Data were acquired on a 6500+ triple quadrupole QTRAP mass spectrometer in low mass negative mode (Sciex) coupled with an ExionLC (Shimadzu) and a Kinetex C18 (100 mm × 3 mm × 2.6 μm, 100 Å) column (Phenomenex). Data were collected using Analyst 1.7.1 (Sciex) and analyzed and presented as screen captures using Sciex OS-Q version 1.7.0.36606 (Sciex). Solvents, gradients, multiple reaction monitoring (MRM), enhanced product ion (EPI) scan settings, and library search parameters, were previously described (41). LibraryView version 1.4 (Sciex) was used to generate a custom metabololipidomics spectral library. Mediator identification criteria required an unbiased spectral

library fit ≥70% and matching retention time to synthetic materials. Synthetic materials were run with each experiment to obtain retention times. The default values of 0.00th for m/z are depicted in figures. However, the accuracy of this instrument is approximately ±*m/z* 0.1. See *SI Appendix*, Table S1 for Q1 (*m/z*), Q3 (*m/z*), dwell time, collision energy, declustering potential, entrance potential, collision cell exit potential, and calibration coefficient for each mediator.

Graft Function Assessment. Two hours after lung transplantation, mice were anesthetized, intubated, and connected to the ventilator. Lungs were ventilated with a fraction of inspired oxygen of 1.0 and exposed by a sternectomy. After a 4-min occlusion of the right hilum, arterial blood was drawn from the left ventricle. Blood gases were measured using an iSTAT Portable Clinical Analyzer (iMale STAT Corp.).

Two-Photon Microscopy. Lung grafts were imaged by intravital two-photon microscopy for periods up to 2 h, as previously described (3). Mice were anesthetized with an intraperitoneal injection of ketamine (50 mg/kg) and xylazine (10 mg/kg) and intubated orotracheally with a 20-G angiocatheter. Mice were ventilated with room air at a rate of 120 breaths per minute with a tidal volume of 0.5 mL. Lung grafts were exposed through a left thoracic window between the third and seventh ribs and imaged with a custom two-photon microscope using ImageWarp or SlideBook acquisition software (A&B Software: Intelligent Imaging Innovations). Then, 15 μL of 655-nm nontargeted Q-dots, suspended in 60 μL of phosphate buffered saline (PBS) were injected intravenously to label blood vessels. For time-lapse imaging we averaged 22 video-rate frames (0.75 s per slice) during the acquisition. Each plane represents an image of 220 × 240 μm in the x and y dimensions. Up to 21 sequential planes were acquired in the z dimension (2.5 μm each) to form a z stack. Percentage of extravasated neutrophils was measured as previously described (6). Intraluminal neutrophil crawling and displacement (distance traveled from site of initial adherence to site of transmigration) were determined as described (24, 25). Multidimensional rendering was done with Imaris (Bitplane), whereas manual cell tracking was performed by using velocity (Improvision). Data were transferred and plotted in Graph Pad Prism 6.0 (Sun Microsystems) for analysis and creation of the graphs.

ELISA. LTB_4 levels in graft tissue homogenates were measured using a commercially available enzyme-linked immunosorbent assay (ELISA) kit (Cayman Chemical) according to the manufacturer's instructions. The ELISA plate was processed using a Synergy HTX Multi-Mode Reader (BioTek).

Flow Cytometry. Graft tissue was digested and single-cell suspensions were prepared as previously reported (6). Following red blood cell lysis, cells were stained with fluorochrome-labeled antibodies against CD45.2 (clone 104; Biolegend), CD45.1 (clone A20; Biolegend), Ly6G (clone 1A8; Thermo Fisher Scientific), CD11b (clone M1/70; Thermo Fisher Scientific), Ly6C (clone HK1.4; Thermo Fisher Scientific), CD115 (clone AFS98; Thermo Fisher Scientific), and isotype control antibodies (BD Biosciences; BioLegend). Data were acquired on an Attune NxT Acoustic Focusing Cytometer (Thermo Fisher Scientific) and analyzed with FlowJo v10 software.

Flow Cytometric Sorting for Single-Cell RNA Sequencing. Recipient mice were treated with RvD1 cocktail or control vehicle intravenously immediately before transplantation. Transplanted left lungs from two mice were collected 2 h postreperfusion and pooled for submission of each sample. Lung tissue was digested, and single-cell suspensions were prepared as previously described (4). Cells were then stained using DAPI (BD Biosciences, #564907) and sorted by flow cytometry for $CD45^+$ leukocytes into 250 μL cell resuspension buffer (0.04% BSA in PBS). Collected cells were centrifuged (300 rcf for 5 min at 4 °C) and resuspended in collection buffer to a target concentration of 1,000 cells/μL. Cells were counted on a hemocytometer before proceeding.

Single-Cell RNA Sequencing Library Preparation. Single-cell suspensions were submitted to the Genome Technology Access Center core facility (Washington University in St. Louis) for single-cell GEM construction and cDNA synthesis and library construction of vehicle- and RvD1-treated lungs. Samples were processed using the Chromium Single Cell 3′ Library & Gel Bead Kit (10X Genomics, v3) following the manufacturer's protocol. The libraries were sequenced on NovaSeq S4 (Illumina) targeting 50,000 reads per cell and 500 million read pairs per library. Cells were aligned to the mouse mm10-2020-A transcriptome using CellRanger (10× Genomics, v6.1.1) to generate feature-barcoded count matrices.

Single-Cell RNA Sequencing Analysis Pipeline. Analysis was performed using the R Seurat v4.0.0 package. The following quality control steps were performed to filter the count matrices: 1) Cells expressing fewer than 500 genes were removed; 2) cells expressing over 6,000 genes were discarded as these could be potential multiplet events where more than a single cell was encapsulated within the same barcoded GEM; 3) cells with >5% mitochondrial content were filtered out as these were deemed to be of low-quality (42). Normalization and variance-stabilization of raw counts was performed using SCTransform, and cell cycle scores were computed and regressed out in combination with percentage mitochondrial reads (43). The normalized R object was then used for subsequent clustering and differential expression testing. Briefly, clusters were annotated into major cell populations, each major cell type was subsetted, and renormalized, PCA, Uniform Manifold Approximation and Projection (UMAP) embedding, clustering, and DE analysis performed. Clusters which resembled low-quality cells or doublets were removed from subsequent analysis. We then computed the principal components and used these to integrate all samples with harmony (44). Informed by the ElbowPlot, we used 50 components to construct the UMAP embedding, find nearest neighbors, and clustered the data at multiple resolutions. We then used the FindAllMarkers function in Seurat to perform differential expression testing and annotated clusters into distinct cell types based on canonical gene markers. We identified a single population that represented a stromal contaminant consistent with vascular endothelium, which was excluded from further analysis. To identify genetic changes induced by treatment, major cell populations were subsetted, renormalized, reclustered, recomputed the UMAP, and differential gene expression analyzed. All differential gene expression used to identify cell types was performed using the normalized assay with the FindAllMarkers function and the Wilcoxon rank sum test with a min.pct = 0.1 and logfc.threshold = 0.25. Differential gene expression of violin plots for individual genes between treatment groups was performed using pairwise comparisons using Wilcox test through the ggpubr package. For pathway analysis, differentially down-regulated genes in RvD1-treated compared to vehicle-treated lungs were used if $P < 0.05$ and $Log_2FC > 0.58$ and analyzed by MSigDB Hallmark 2020 Pathway analysis (https://maayanlab.cloud/Enrichr).

Statistics. Data were analyzed by Prism version 7.0d. For the comparison of two groups, data were analyzed with the two-tailed unpaired *t* test. For multiple group comparisons, we tested for normality (Shapiro–Wilks test) and data were analyzed by Kruskal–Wallis test. A *P* value of less than 0.05 was considered significant.

Data, Materials, and Software Availability. Code from scRNAseq data can be found on github:https://github.com/hmshepherd/ResolvinD1 (45). The sequences have been deposited in the Gene Expression Omnibus (GEO) database (https://www.ncbi.nlm.nih.gov/geo/) (accession no. GSE237110) (46). All other data are included in the article and/or supporting information.

ACKNOWLEDGMENTS. C.N.S. is supported by the NIH/NIGMS R35 GM139430. D.K. is supported by NIH grants 1P01AI116501, R01HL094601, R01HL151078, and U01163086-01, Veterans Administration Merit Review grant 1I01BX002730, and The Foundation for Barnes-Jewish Hospital.

Author affiliations: [a]Division of Cardiothoracic Surgery, Department of Surgery, Washington University in St. Louis, St. Louis, MO 63110; [b]Department of Anesthesiology, Perioperative, and Pain Medicine, Center for Experimental Therapeutics and Reperfusion Injury, Brigham and Women's Hospital and Harvard Medical School, Boston, MA 02115; [c]Department of Medicine, Washington University in St. Louis, St. Louis, MO 63110; and [d]Department of Pathology and Immunology, Washington University in St. Louis, St. Louis, MO 63110

Author contributions: W.L., H.M.S., Y.T., A.E.S., A.E.G., K.J.L., C.N.S., and D.K. designed research; W.L., H.M.S., Y.T., A.E.S., and A.I.B. performed research; W.L., H.M.S., Y.T., A.E.S., A.E.G., K.J.L., C.N.S., and D.K. analyzed data; and W.L., H.M.S., C.N.S., and D.K. wrote the paper.

Competing interest statement: Resolvins are biotemplates for stable analogs. Patents on these are awarded and assigned to the Brigham and Women's Hospital, and C.N.S. is the inventor. These analog patents are licensed for clinical development. K.J.L. and D.K. have a pending patent entitled "Compositions and methods for detecting CCR2 receptors" (application No. 15/611,577).

1. G. I. Snell *et al.*, Report of the ISHLT Working Group on Primary Lung Graft Dysfunction, part I: Definition and grading-A 2016 Consensus Group statement of the International Society for Heart and Lung Transplantation. *J. Heart Lung Transplant* **36**, 1097–1103 (2017).
2. W. Li *et al.*, Necroptosis triggers spatially restricted neutrophil-mediated vascular damage during lung ischemia reperfusion injury. *Proc. Natl. Acad. Sci. U.S.A.* **119**, e2111537119 (2022).
3. D. Kreisel *et al.*, In vivo two-photon imaging reveals monocyte-dependent neutrophil extravasation during pulmonary inflammation. *Proc. Natl. Acad. Sci. U.S.A.* **107**, 18073–18078 (2010).
4. Z. Zheng *et al.*, Donor pulmonary intravascular nonclassical monocytes recruit recipient neutrophils and mediate primary lung allograft dysfunction. *Sci. Transl. Med.* **9**, eaal4508 (2017).
5. C. Kurihara *et al.*, Crosstalk between nonclassical monocytes and alveolar macrophages mediates transplant ischemia-reperfusion injury through classical monocyte recruitment. *JCI Insight* **6**, e147282 (2021).
6. H. M. Hsiao *et al.*, Spleen-derived classical monocytes mediate lung ischemia-reperfusion injury through IL-1beta. *J. Clin. Invest.* **128**, 2833–2847 (2018).
7. D. Kreisel *et al.*, Emergency granulopoiesis promotes neutrophil-dendritic cell encounters that prevent mouse lung allograft acceptance. *Blood* **118**, 6172–6182 (2011).
8. C. N. Serhan, Pro-resolving lipid mediators are leads for resolution physiology. *Nature* **510**, 92–101 (2014).
9. A. Hopke *et al.*, Transcellular biosynthesis of leukotriene B(4) orchestrates neutrophil swarming to fungi. *iScience* **25**, 105226 (2022).
10. S. E. Malawista, A. de Boisfleury Chevance, J. van Damme, C. N. Serhan, Tonic inhibition of chemotaxis in human plasma. *Proc. Natl. Acad. Sci. U.S.A.* **105**, 17949–17954 (2008).
11. H. Luan *et al.*, Resolvin D1 protects against ischemia/reperfusion-induced acute kidney injury by increasing Treg percentages via the ALX/FPR2 pathway. *Front. Physiol.* **11**, 285 (2020).
12. V. Kain *et al.*, Resolvin D1 activates the inflammation resolving response at splenic and ventricular site following myocardial infarction leading to improved ventricular function. *J. Mol. Cell Cardiol.* **84**, 24–35 (2015).
13. V. Leroy *et al.*, Resolution of post-lung transplant ischemia-reperfusion injury is modulated via Resolvin D1-FPR2 and Maresin 1-LGR6 signaling. *J. Heart Lung Transplant.* **42**, 562–574 (2022), 10.1016/j.healun.2022.12.013.
14. H. Oda *et al.*, Specialized proresolving lipid meditators agonistic to formyl peptide receptor Type 2 attenuate ischemia-reperfusion injury in rat lung. *Transplantation* **106**, 1159–1169 (2022).
15. G. Fredman *et al.*, Resolvin D1 limits 5-lipoxygenase nuclear localization and leukotriene B4 synthesis by inhibiting a calcium-activated kinase pathway. *Proc. Natl. Acad. Sci. U.S.A.* **111**, 14530–14535 (2014).
16. T. Chtanova *et al.*, Dynamics of T cell, antigen-presenting cell, and pathogen interactions during recall responses in the lymph node. *Immunity* **31**, 342–355 (2009).
17. M. Okazaki *et al.*, A mouse model of orthotopic vascularized aerated lung transplantation. *Am. J. Transplant.* **7**, 1672–1679 (2007).
18. D. Van Raemdonck *et al.*, Donation after circulatory death in lung transplantation-five-year follow-up from ISHLT Registry. *J. Heart Lung. Transplant.* **38**, 1235–1245 (2019).
19. S. Krishnamoorthy *et al.*, Resolvin D1 binds human phagocytes with evidence for proresolving receptors. *Proc. Natl. Acad. Sci. U.S.A.* **107**, 1660–1665 (2010).
20. J. F. Markworth *et al.*, Human inflammatory and resolving lipid mediator responses to resistance exercise and ibuprofen treatment. *Am. J. Physiol. Regul. Integr. Comp. Physiol.* **305**, R1281–R1296 (2013).
21. B. D. Levy, C. B. Clish, B. Schmidt, K. Gronert, C. N. Serhan, Lipid mediator class switching during acute inflammation: Signals in resolution. *Nat. Immunol.* **2**, 612–619 (2001).
22. B. Petri, M. Phillipson, P. Kubes, The physiology of leukocyte recruitment: An in vivo perspective. *J. Immunol.* **180**, 6439–6446 (2008).
23. M. Dona *et al.*, Resolvin E1, an EPA-derived mediator in whole blood, selectively counterregulates leukocytes and platelets. *Blood* **112**, 848–855 (2008).
24. M. Phillipson *et al.*, Intraluminal crawling of neutrophils to emigration sites: A molecularly distinct process from adhesion in the recruitment cascade. *J. Exp. Med.* **203**, 2569–2575 (2006).
25. W. Li *et al.*, Intravital 2-photon imaging of leukocyte trafficking in beating heart. *J. Clin. Invest.* **122**, 2499–2508 (2012).
26. H. Kim *et al.*, TNF-alpha-induced up-regulation of intercellular adhesion molecule-1 is regulated by a Rac-ROS-dependent cascade in human airway epithelial cells. *Exp. Mol. Med.* **40**, 167–175 (2008).
27. A. K. Sharma, L. G. Fernandez, A. S. Awad, I. L. Kron, V. E. Laubach, Proinflammatory response of alveolar epithelial cells is enhanced by alveolar macrophage-produced TNF-alpha during pulmonary ischemia-reperfusion injury. *Am. J. Physiol-Lung. C* **293**, L105–L113 (2007).
28. J. H. Spahn *et al.*, DAP12 expression in lung macrophages mediates ischemia/reperfusion injury by promoting neutrophil extravasation. *J. Immunol.* **194**, 4039–4048 (2015).
29. T. Lammermann *et al.*, Neutrophil swarms require LTB4 and integrins at sites of cell death in vivo. *Nature* **498**, 371-+ (2013).
30. H. M. Hsiao *et al.*, Resolvin D1 reduces emphysema and chronic inflammation. *Am. J. Pathol.* **185**, 3189–3201 (2015).
31. H. W. Zhang *et al.*, RvD1 ameliorates LPS-induced acute lung injury via the suppression of neutrophil infiltration by reducing CXCL2 expression and release from resident alveolar macrophages. *Int. Immunopharmacol.* **76**, 105877 (2019).
32. R. E. Abdulnour *et al.*, Aspirin-triggered resolvin D1 is produced during self-resolving gram-negative bacterial pneumonia and regulates host immune responses for the resolution of lung inflammation. *Mucosal. Immunol.* **9**, 1278–1287 (2016).
33. M. Sekheri, D. El Kebir, N. Edner, J. G. Filep, 15-Epi-LXA4 and 17-epi-RvD1 restore TLR9-mediated impaired neutrophil phagocytosis and accelerate resolution of lung inflammation. *Proc. Natl. Acad. Sci. U.S.A.* **117**, 7971–7980 (2020).
34. P. C. Norris, D. Gosselin, D. Reichart, C. K. Glass, E. A. Dennis, Phospholipase A2 regulates eicosanoid class switching during inflammasome activation. *Proc. Natl. Acad. Sci. U.S.A.* **111**, 12746–12751 (2014).
35. T. Liu *et al.*, HMGB1-C1q complexes regulate macrophage function by switching between leukotriene and specialized proresolving mediator biosynthesis. *Proc. Natl. Acad. Sci. U.S.A.* **116**, 23254–23263 (2019).
36. H. S. Kulkarni *et al.*, Local complement activation is associated with primary graft dysfunction after lung transplantation. *JCI Insight* **5**, e138358 (2020).
37. Z. Hosseini *et al.*, Resolvin D1 enhances necroptotic cell clearance through promoting macrophage fatty acid oxidation and oxidative phosphorylation. *Arterioscl. Throm. Vas.* **41**, 1062–1075 (2021).
38. M. Spinosa *et al.*, Resolvin D1 decreases abdominal aortic aneurysm formation by inhibiting NETosis in a mouse model. *J. Vasc. Surg.* **68**, 93S–103S (2018).
39. C. N. Serhan, N. Chiang, T. E. Van Dyke, Resolving inflammation: Dual anti-inflammatory and pro-resolution lipid mediators. *Nat. Rev. Immunol.* **8**, 349–361 (2008).
40. N. Chiang *et al.*, Infection regulates pro-resolving mediators that lower antibiotic requirements. *Nature* **484**, 524–528 (2012).
41. A. E. Shay *et al.*, Human leukocytes selectively convert 4S,5S-epoxy-resolvin to resolvin D3, resolvin D4, and a cys-resolvin isomer. *Proc. Natl. Acad. Sci. U.S.A.* **118**, e2116559118 (2021).
42. D. Osorio, J. J. Cai, Systematic determination of the mitochondrial proportion in human and mice tissues for single-cell RNA-sequencing data quality control. *Bioinformatics* **37**, 963–967 (2021).
43. C. Hafemeister, R. Satija, Normalization and variance stabilization of single-cell RNA-seq data using regularized negative binomial regression. *Genome Biol.* **20**, 296 (2019).
44. I. Korsunsky *et al.*, Fast, sensitive and accurate integration of single-cell data with Harmony. *Nat. Methods* **16**, 1289–1296 (2019).
45. W. Li, H. M. Shepherd, K. J. Lavine, D. Kreisel. RvD1 Lung scRNAseq. GitHub. https://github.com/hmshepherd/ResolvinD1. Deposited 9 July 2023.
46. W. Li, H. M. Shepherd, K. J. Lavine, D. Kreisel. Single cell RNA-seq analysis of immune cells in vehicle- and RvD1-treated murine lung grafts. NCBI GEO. https://www.ncbi.nlm.nih.gov/geo/query/acc.cgi?acc=GSE237110. Deposited 12 July 2023.